

Planar Light Valve Optical Head for High Throughput 10 μ m Feature Size Laser Processing

Gregory Jacob*, Hirofumi Mizuno, Tianbo Liu, Alex Payne, and Lars Eng

Silicon Light Machines, USA

*Corresponding author's e-mail: gjacob@siliconlight.com

A high-throughput laser micro-machining system has been developed using a programmable multi-spot modulated line beam capable of >30x throughput enhancement over a single-spot system. While commercially available lasers have been rapidly growing in output energy and power, single-spot scanning systems cannot take full advantage of these advancements. This system provides high throughput, high resolution micro-processing on a variety of surfaces (stainless steel, aluminum, and polymer). This high productivity system is enabled by a high-power MEMS spatial light modulator called the Planar Light Valve (PLVTM). The PLV is a 1088-pixel device in a linear configuration capable of 10-bit, 100 kHz amplitude modulation. The PLV supports pulse energies of ~1 mJ (1064 nm, 10 ps) and has been used at pulse widths down to 300 femtoseconds. The system can resolve features as small as 10 μ m with an edge placement resolution of 2.5 μ m. Large area processing is done by scanning and stitching this line beam across the media using X-Y stages and a unique relay galvo scanner has been incorporated into the system to allow for faster scanning over a 15 x 15 mm area.

DOI: 10.2961/ilmn.2024.02.2006

Keywords: PLV, multi-beam, spatial light modulator, high power, scan head, MEMS

1. Introduction

1.1 Laser processing systems

Many manufacturing processes rely on lasers for their precision and speed [1-6]. There is a widespread need for higher throughput systems to meet customer demands and reduce the cost of producing parts. A typical laser processing system consists of a collimated laser beam scanned by galvo mirrors and focused through an f-theta lens. As laser powers and pulse energies have continued to grow, the single-spot system cannot take full advantage of the laser output energy, especially when high resolution is required [7]. The highest-performance galvo scanners can scan at speeds of 30 m/s and polygon scanners can scan as fast as 90 m/s [8]. But even a 90m/s scan speed can only utilize a 50W laser with a 10 μ m spot size. This means that higher-power lasers cannot be used to their full potential or are restricted to larger spot sizes which limits their application to lower-resolution applications.

1.2 Multi-beam system architecture

Laser processing systems have begun using multiple beams to increase the throughput [9-12]. While the beam scanning and delivery system can be replicated to create multiple beams, this leads to complex software control to divide up the processing work and create seamless interfaces. This approach also has limitations in scalability. In this paper a more scalable approach is taken of splitting the beam into many spots that can be modulated at high speed [13,14]. The resulting system requires much slower scan speeds and can easily take advantage of higher repetition rates and average powers of lasers. To make use of higher pulse energy, a straightforward optical magnification

change is required if the output fluence is to be kept constant.

A spatial light modulator (SLM) is used to enable on-the-fly pattern switching of incident laser light [15-18]. To be performant in high-power applications, the SLM must have a suitable damage threshold and operate at kHz switching rates. The Planar Light Valve (PLVTM) was chosen for this system because it can support pulse energies of up to 920 μ J at 200 fs duration. It can operate in the wavelength range of 355 – 1070 nm and supports switching speeds of >100 kHz [13,19].

1.3 Planar Light Valve Spatial Light Modulator

The PLV is a MEMS device composed of a tiled array of circular pistons enclosed by a static faceplate. In the short axis, 40 pistons are ganged electrically to make a 1,020 μ m tall pixel. The long axis contains 1,088 pixels which are the width of a single element (25.5 μ m) for a total length of 27.7 mm (Figure 1) [19].

Similar to the Grating Light Valve (GLV), the PLV utilizes a diffraction mechanism to modulate light by directing it into different diffraction orders which are either passed or dumped depending on the order (Figure 2) [20,21]. When no voltage is placed on the dynamic faceplates, they are level with that static portion and create a mirror-like surface. When a voltage is placed on the dynamic portion (shown in red) it is drawn toward the common baseplate below by a capacitive force, creating a variable depth diffraction grating. The light that reflects off the dynamic and static portions will destructively interfere and create diffraction orders. Input light picks up a round-trip phase shift equal to twice the displacement, thus the maximum interference will occur when at a displacement of $\lambda/4$, where λ

is the wavelength of the light. The optical system is arranged in such a way that light reflected into the 0th order is passed, while light diffracted into higher orders is blocked by a spatial filter. In this way, the displacement of a face-plate translates to intensity modulation in the image plane. The highest intensity in the image plane is seen at 0 displacement and the lowest intensity (dark state) is seen at $\lambda/4$ displacement. The voltage and resulting displacement is controlled with 10-bit resolution on each channel, which allows for 1,024 intensity values in the image plane for each pixel.

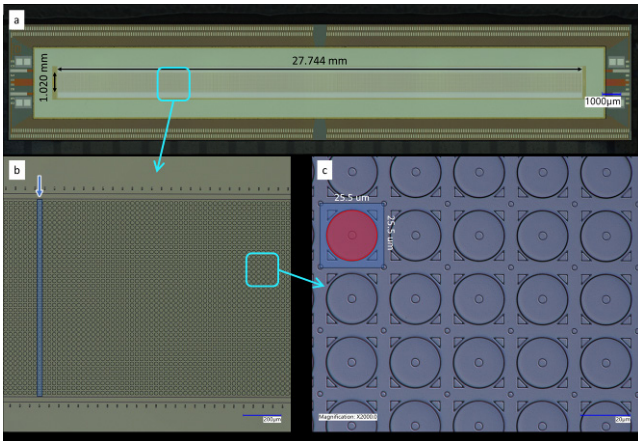


Fig. 1 Images of the PLV device showing (a) the entire device die, (b) a zoomed-in section of the optical area with one device pixel highlighted (1 element wide by 40 elements tall), and (c) a further zoomed-in section showing individual elements with the dynamic part highlighted in red.

It has a large optical area since the full 40-element length of each pixel can be used to modulate light. Light is spread out over the entire device to keep the power density low and condensed into a thin line at the work surface.

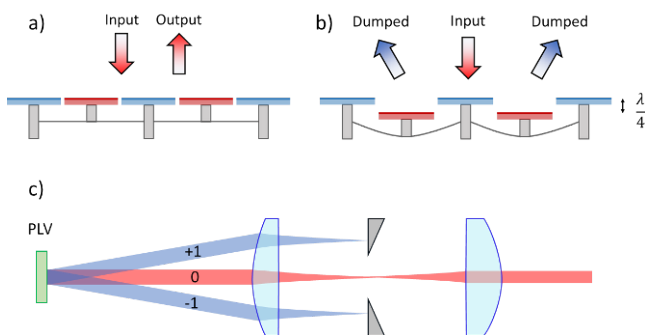


Fig. 2 Illustration showing (a) device with maximum light going to 0th order, (b) maximum light going to 1st orders, and (c) an example optical system with a spatial filter cutting off the 1st orders.

1.4 Optical Head

The optical head was designed as a turn-key solution to quickly start working with a PLV-modulated multi-spot beam. It provides high-quality beam shaping and imaging optics in an industrial enclosure, allowing users to focus on laser processing rather than optical implementation.

2. Methodology

2.1 Optical system

The optical system consists of illumination optics, projection optics, and relay optics (Figure 3). The illumination optics take a Gaussian beam input from the laser and create a rectangular beam at the PLV with a top-hat profile in both dimensions. The beam expander is used to resize the beam to a diameter of 5 mm for the top-hat shaper. The top-hat shaper and focusing lens create a 4 x 4 mm square top-hat beam. The cylindrical telescope resizes the square top-hat beam into a 27 x 1 mm top-hat to match the dimensions of the PLV. This telescope comprises 3 lenses for the short-axis and 3 lenses for the long-axis to precisely control the dimensions of the beam on the PLV.

The projection optics create an anamorphic image of the PLV which is imaged by the galvo relay system to the work surface. The long-axis is imaged with a demagnification of 10.4x, so the pattern on the PLV can be seen at the intermediate image plane as well as at the final output image. The short-axis is focused as tightly as possible to a 10 μm focus with a sinc² profile. A pickoff mirror sends a small amount of light to the calibration system, which is used to measure and flatten out any nonuniformities in the illumination. The result is a flat-top line beam that is 2.5 mm long with $\sim 10 \mu\text{m}$ sinc² profile in the short axis (Figure 4). At any moment, the pattern displayed on the PLV is the pattern that is seen at the work surface, making it intuitive to place energy exactly where it is needed.

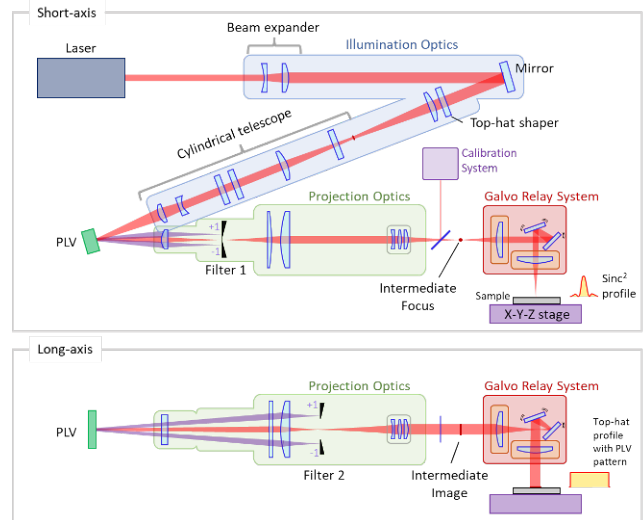


Fig. 3 Schematic of the optical system used in the PLV optical head.

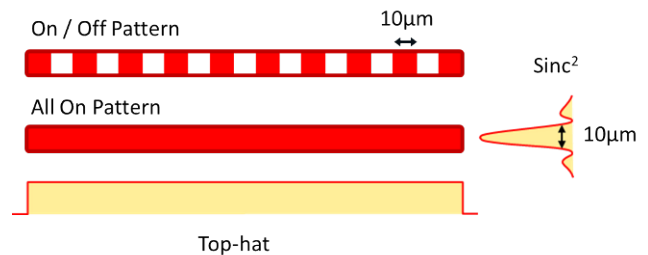


Fig. 4 Optical head output beam with example on/off pattern and all on pattern.

The turn-key version of this system utilizes an integrated 100 W, 460 μ J, 10 ps, 1064 nm laser. It can also be used with many other lasers by coupling the light in through an input window.

2.2 Scanning over media

The PLV provides modulation in the long axis of the line beam. To process a 2D structure the line beam must be scanned orthogonally to the modulation direction. As the beam is scanned the pattern is changed to deposit energy where it is required. The scanning motion can be achieved by moving the beam or by moving the media. Many types of scanners can be used by themselves or in conjunction with others. Examples include stages, galvo mirrors, roll-to-roll, rotating drum, and spinning disk to name a few.

2.3 Galvo relay optics

The optical head employs a unique integrated galvo scanning relay system. Whereas a single-spot system needs only to scan and focus a beam, the galvo relay optics used here are designed to image and scan the PLV pattern to the work surface (Figure 5). Two identical f-theta lenses were used with a separation of 50 mm to create a 1x magnification relay system. The imaging configuration is key to enabling the use of galvos in the system. A focal length of 65 mm was chosen for the f-theta lens to be able to resolve 10 μ m features. This results in a scan field of 15 x 15 mm. Stages with a longer travel can be used for processing larger areas.

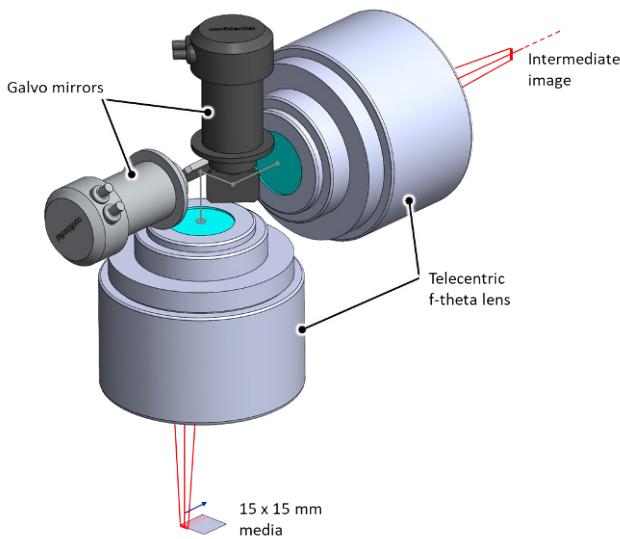


Fig. 5 Galvo relay system which images and scans the intermediate line beam image.

2.4 Motion synchronization

The scanning motion must be synchronized with the PLV pattern to deposit energy in the desired locations. If the pattern being processed is wider than the line beam, the beam is scanned over the area in multiple passes (Figure 6). A demo system has been built that can scan the workpiece using XY stages or scan the beam using the integrated galvos.

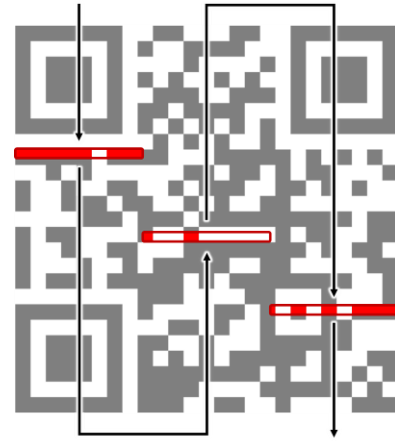


Fig. 6 Example of scan path used when more than one pass is needed to cover the processing area.

When using XY stages the position encoder signals from the scanning stage are used to create a trigger signal to advance the pattern (also called the column) of the PLV (Figure 7). In this way, the PLV pattern can be synchronized with the position of the stages.

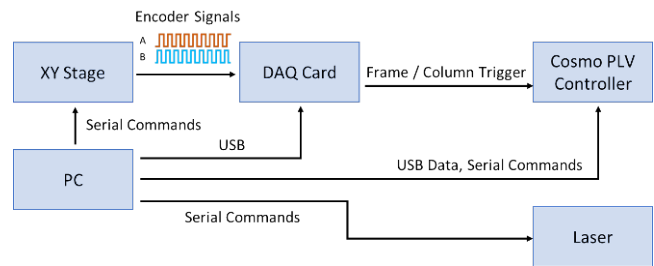


Fig. 7 Schematic of signals used for synchronization with stage scanning.

When using the galvo mirrors a signal is sent from the galvo controller at the start of the scan (Figure 8). The PLV controller will then run a collection of patterns (called a frame) at a pre-defined period set on an internal clock.

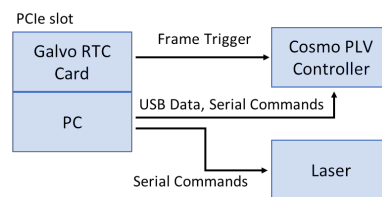


Fig. 8 Schematic of signals used for synchronization with galvo scanning.

2.5 Distortion compensation

One challenge when working with galvos is the distortion that is introduced by the f-theta lens. Ideally, the beam would be scanned in a straight line when only one axis is in motion. However, the straight scan paths become curved due to barrel distortion, and the scans overlap more the farther away from the center we go (Figure 9).

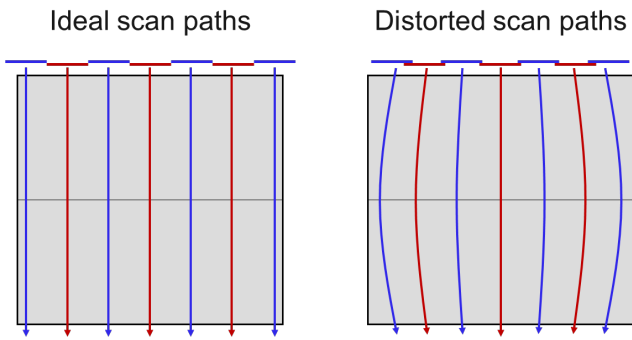


Fig. 9 Illustration showing ideal scan paths and the scan paths after being distorted by the f-theta lens.

With a single beam, this could be corrected in the galvo controller. When scanning the multi-spot line beam in this system, extra complexity is introduced because the distortion can vary across the line. One approach to compensate for the distortion is to use distortion data to pre-distort the input pattern so that a non-distorted pattern results after processing (Figure 10).

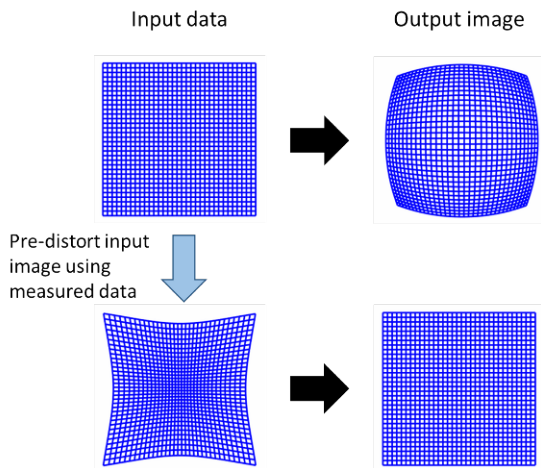


Fig. 10 Illustration showing the concept of pre-distorting the image to compensate for the inherent distortion in the f-theta lens. Images from <https://learnopencv.com/understanding-lens-distortion/>

A matrix of distortion data is required to calculate the pre-distorted image. A denser matrix will lead to more accurate distortion correction, but getting data at each pixel of the input image is not possible. So, the data is calculated for each pixel is calculated using bilinear interpolation. Each pixel in the input image is mapped to a new pixel in the distorted image. For example, consider a certain pixel with measured distortion of $-9 \mu\text{m}$ in X and $-10 \mu\text{m}$ in Y where each pixel represents $5 \mu\text{m}$. This pixel would then be shifted $+2$ pixels in X (rounding to the nearest pixel) and $+2$ pixels in Y when creating the distorted image. After all pixels are mapped to their new location, some holes are left in the image. For high-contrast binary images these holes can simply be filled in by averaging the 4 nearest neighbor pixels. For gray-scale images, a different method may be required.

3. Data and Results

3.1 Resolution

The feature size in the PLV-modulated direction can be adjusted by setting groups of pixels to the on state (maximum intensity) and the off state (minimum intensity). In Figure 11 black-marked features are shown for blocks of 12 pixels on, 12 pixels off down to 1 pixel on, 1 pixel off. The marks created appear well-resolved down to 4 pixels, corresponding to a $9.8 \mu\text{m}$ beam size. The measured feature size will depend on the application and laser parameters being used. When using 3 pixels or less, the spatial frequencies exceed the resolution of the optics and we see lower contrast marks.

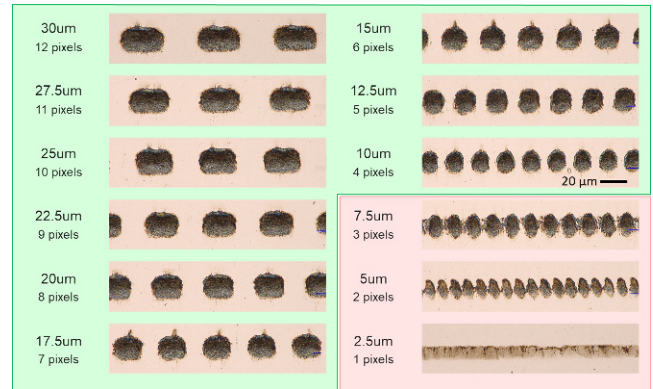


Fig. 11 Black-marked features on SS304 showing well-resolved spots down to a grouping of 4 PLV pixels.

The horizontal and vertical resolutions were also tested against scan speed. Figure 12 shows vertical lines made with blocks of 4 pixels on, and 4 pixels off. Multiple passes were used at higher scan speeds to darken the image. This pattern shows well-resolved lines and spaces even at the highest scan speed of 854 mm/s .

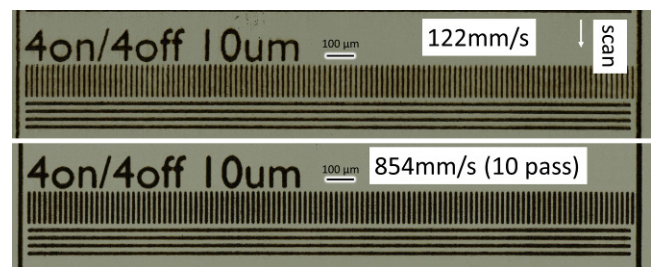


Fig. 12 Horizontal and vertical line pairs created at different scan speeds. Well-resolved vertical lines from the PLV pattern are seen throughout.

Figure 13 shows horizontal lines made by turning the entire PLV array on and off. The modulation frequency is noted at the left of each image. We see well-resolved lines up to 117 kHz , but at 150 kHz the lines become significantly lighter indicating that the PLV may not have fully reached the on state. In this test, the modulation rate is increased by increasing the scan speed. This also leads to lighter features because fewer pulses hit a given area. Thus, this result should be taken as a rough characterization of the modulation rate of the PLV

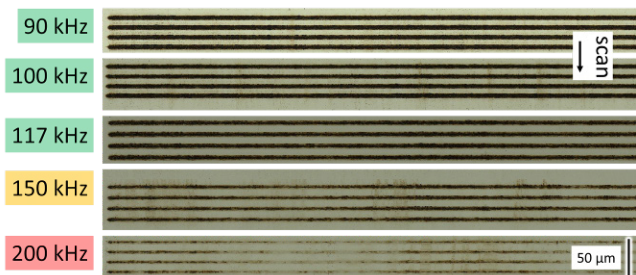


Fig. 13 Horizontal lines created at increasing modulation frequencies by setting the PLV to all pixels on state and all pixels off state.

3.2 Edge placement

The edge placement capabilities work with the resolution to determine how smoothly laser-marked features are rendered. Though the optics can resolve features as small as 4 PLV pixels, these features can be shifted to adjacent pixels on the array in steps of 1 pixel. Effectively we have a grid set at 2.5 μm on which we place the spots in our line beam, allowing us to create very smooth diagonal features (Figure 14).

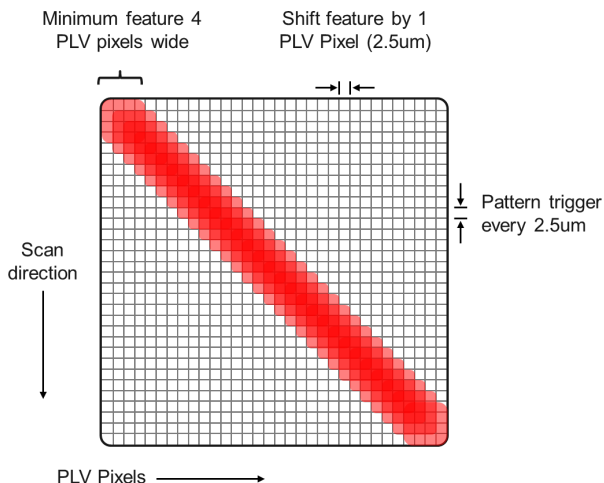


Fig. 14 Illustration showing how shifting a spot by 1 PLV pixel as the pattern increments results in smoothly rendered diagonal features.

Different grid sizes were used to mark a sample image shown in Figure 15. A staircase effect is seen at the coarser grid sizes, but the finer grid sizes show very smooth features. The processing time is the same regardless of grid size. The only penalties are that more data and higher triggering frequency are required at finer grid sizes. For black marking on stainless steel, a typical scan rate of 40 mm/s with a 2.5 μm grid size requires a trigger frequency of 16 kHz, which is well within the capabilities of the PLV.

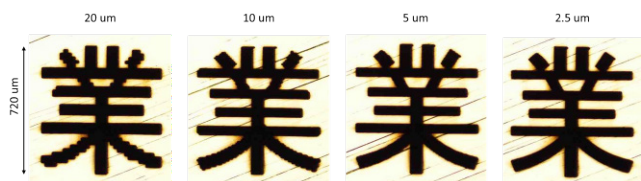


Fig. 15 Example showing the effect of marking the same image at different grid sizes.

3.3 Distortion correction

The distortion was measured by marking 100 μm diameter spots at a 500 μm pitch across the entire scan field. The actual position was located and plotted against the ideal position (Figure 16). The difference between these two points is the distortion.

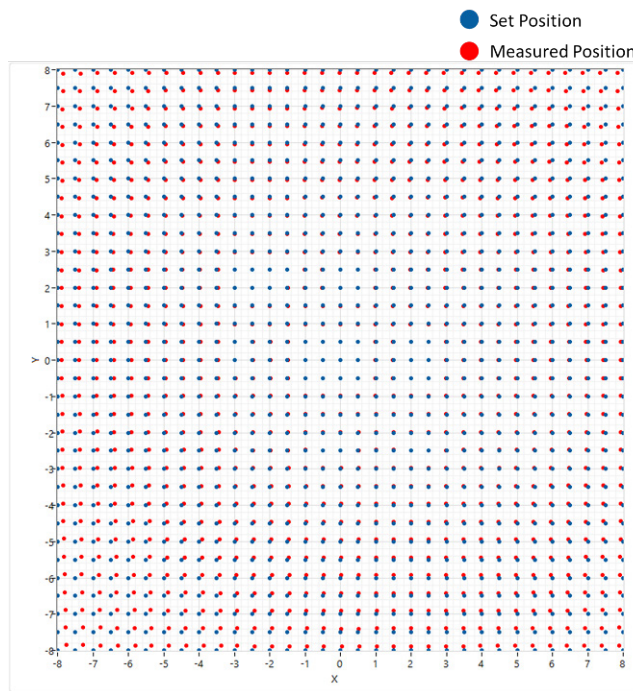


Fig. 16 Distortion data collected over 16 x 16 mm area.

Using the method of pre-distorting the image discussed in section 2.5, a square image was marked with and without distortion correction shown in Figure 17. The corrected image has noticeably straighter sides than the uncorrected image. Table 1 shows the measurements of the sides of the square images. Before distortion correction, the magnitude of the average error over the length of the 4 sides was 1.29%. This was reduced to 0.13% after distortion correction.

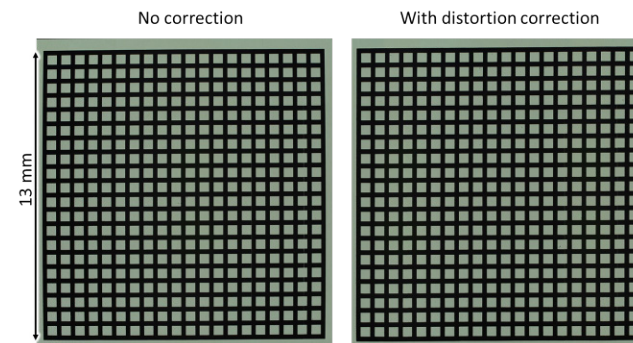


Fig. 17 Square image marked without and with distortion correction.

Table 1 Measurements of square images shown in Figure 17 before and after distortion correction.

| Dimension | Ideal (μm) | Before Correction | | After Correction | |
|--------------|-------------------------|----------------------------|-----------|----------------------------|-----------|
| | | Measured (μm) | Error (%) | Measured (μm) | Error (%) |
| Top Width | 12740 | 12538 | -1.59 | 12767 | 0.21 |
| Bottom Width | 12740 | 12562 | -1.40 | 12748 | 0.06 |
| Left Height | 13000 | 12844 | -1.20 | 13004 | 0.03 |
| Right Height | 13000 | 12873 | -0.98 | 13029 | 0.22 |

The original array of spots was marked with distortion correction, and the average distortion was reduced by 2.2x, from 73 μm to 33 μm (Figure 18). Some of the spots were pushed out too much resulting in a positive displacement error, so this area of distortion correction has an opportunity for further improvement. In future work, it may be possible to correct large-scale distortion errors in the galvo controller and make small corrections by pre-distorting the image, which will help to equalize the overlaps between adjacent passes of the line beam.

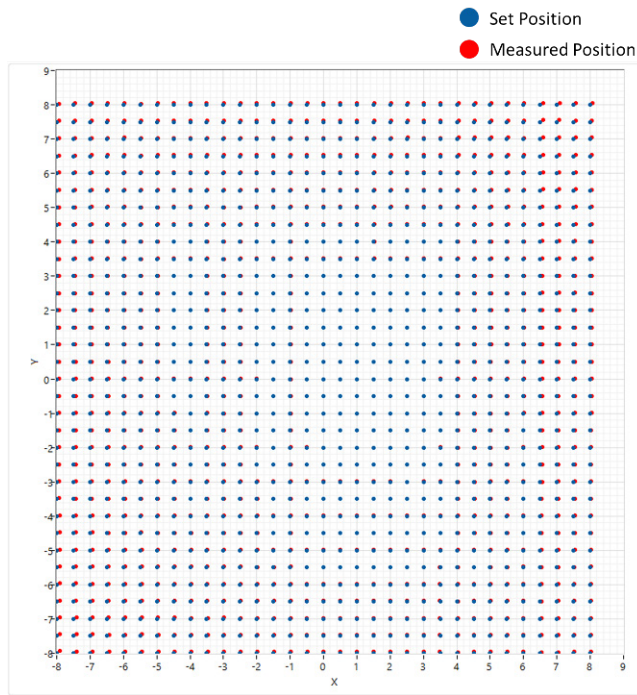


Fig. 18 Location of grid of dots after pre-distorting image.

3.4 Process time

A selection of images was marked on 304 stainless steel to compare against a typical single-spot marking system. The images shown in Figure 19 range from very dense to very sparse with a range of feature sizes.



Fig. 19 Selection of images used for throughput comparison.

Processing times for the single-spot system and PLV multi-spot system are shown in Table 2. The single-spot markings had an L^* of 21.67. The multi-spot system parameters were dialed in to get close to this value with an L^* of 22.82. The L^* is a measure of the darkness of a sample with a value closer to 0 indicating a darker sample. A difference of 2.0 is just noticeable to the human eye, so the darkness of the images generated is very hard to tell apart. The fine features of images 4 and 5 were noticeably sharper on the multi-spot system. For the multi-spot system, a scan speed of 45 mm/s was used with a repetition rate of 400 kHz and laser pulse energy of 233 μJ . The resulting peak fluence at the media was 0.6 J/cm^2 at the center of the short-axis profile.

Table 2 Process times and throughput enhancement for five benchmark images using a single-spot system (50 W, 25 μJ , 3 ps) and the PLV multi-spot system. On the single-spot system, all processing was done with galvo mirrors. On the multi-spot system, images smaller than 15 x 15 mm were processed by scanning the galvo mirrors while larger images were processed by only scanning the stages.

| # | Image Name | Size (mm) | Single-Spot 50W | Multi-spot system 93W | | |
|---|--------------|-------------|-----------------|-----------------------|----------|------------|
| | | | Time (s) | Scanner | Time (s) | Throughput |
| 1 | Black Circle | ϕ 30 | 264.93 | Stage | 14.48 | 18.3x |
| 2 | Dot Matrix | 9.3 x 9.3 | 7.11 | Galvo | 0.72 | 9.9x |
| 3 | QR Code | 10 x 10 | 34.04 | Galvo | 0.97 | 35.1x |
| 4 | SLM Logo | 6.6 x 10 | 14.43 | Galvo | 0.58 | 24.9x |
| 5 | Small Text | 33.4 x 11.4 | 92.01 | Stage | 4.84 | 19.0x |

3.5 Engraving rates

The multi-spot system was also used to demonstrate engraving on stainless steel. Rather than just modifying the surface structure, engraving aims to remove some amount of material. Table 3 below shows the depths ranging from 135 μm to 486 μm and corresponding removal rates.

Table 3 Engraving depths and corresponding removal rates. Laser used was Carbide 1030 nm at 100 kHz, 800 μJ (1.75 J/cm^2 peak fluence), and a scan speed of 5 mm/s was used

| Passes | Depth (μm) | Time (sec) | Depth / pass (μm) | Removal Rate (mm^3/min) |
|--------|-------------------------|------------|--------------------------------|---|
| 33 | 135 | 412.5 | 4.09 | 1.96 |
| 67 | 259 | 837.5 | 3.87 | 1.86 |
| 133 | 486 | 1662.5 | 3.65 | 1.75 |

3.6 Sample images

Figures 20-23 show a small sampling of images and markings created with the optical head.



Fig. 20 Black-marked image on stainless steel of (a) chess board, (b) and (c) zoomed in showing 10 μm wide unmarked outline around the knight.

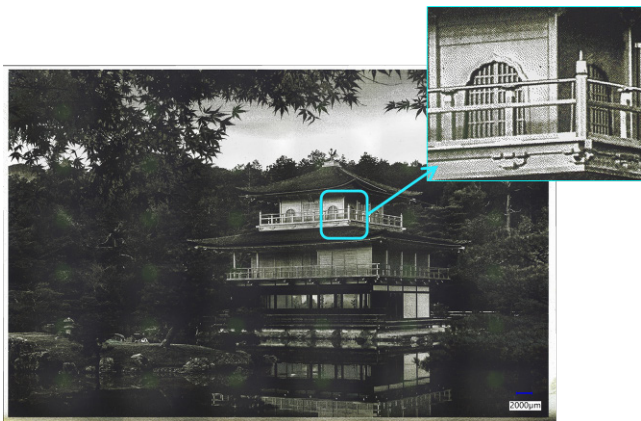


Fig. 21 Golden Palace in Kyoto marked on 68 x 45 stainless steel plaque.



Fig. 22 Images marked on silicon wafers in collaboration with A. Brand, Fraunhofer ISE. Laser used was Photonics Industries RX2 at 90 W power, 200 kHz repetition rate and peak fluence of 1.0 J/cm^2 .

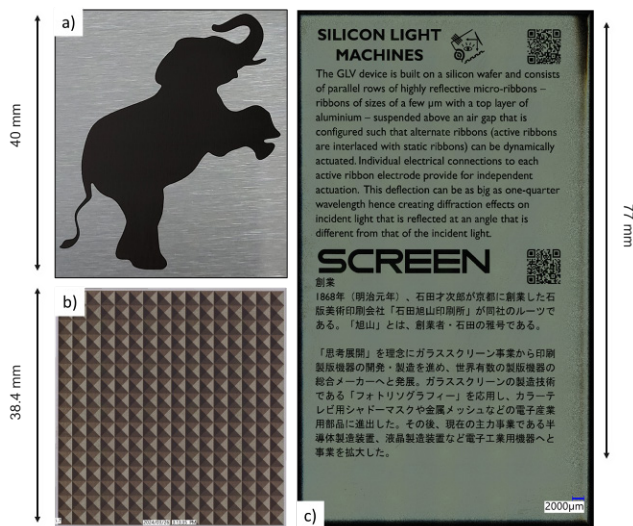


Fig. 23 Images of (a) large black-marked area on stainless steel, (b) visual pyramid effect created with grayscale dithering, and (c) sharp text.

4. Conclusions

An optical head for laser processing has been demonstrated with up to 35x throughput enhancement at $>10\times$ resolution (10 μm feature) compared to a 58 μm single spot system. The throughput can be further scaled with a more powerful laser. This system is especially well-suited for applications with densely marked features at high resolution.

Though a large throughput enhancement has already been demonstrated, new PLV devices are in development which are estimated to provide $>5\times$ throughput enhancement compared to the system discussed here. Other versions of the optical head are also in development to work at different wavelengths (green and UV), as well as to deliver a longer line beam to the media for faster processing.

References

- [1] M. Schmidt, M. Merklein, D. Bourell, D. Dimitrov, T. Hausotte, K. Wegener, L. Overmeyer, F. Vollertsen, and G.N. Levy: *CIRP Ann. Manuf. Technol.*, 66, (2017) 561.
- [2] M. Malinauskas, A. Žukauskas, S. Hasegawa, Y. Hayasaki, V. Mizeikis, R. Buividas, and S. Juodkazis: *Light Sci. Appl.*, 5, (2016) 16133.
- [3] V. Kumar, R. Verma, S. Kango, and V.S. Sharma: *Mater. Today Commun.*, 26, (2021) 101736.
- [4] K. Sugioka and Y. Cheng: *Light Sci. Appl.*, 3, (2014) 149.
- [5] W. Pfleging: *Nanophotonics*, 7, (2018) 549
- [6] M. Duocastella and C.B. Arnold: *Laser Photon. Rev.*, 6, (2012) 607.
- [7] A.F. Sartori, S. Orlando, A. Bellucci, D.M. Trucchi, S. Abrahami, T. Boehme, T. Hantschel, W. Vandervorst, and J.G. Buijnsters: *ACS Appl. Mater. Interfaces*, 10, (2018) 43236.
- [8] T. Lee and H. Haloui: *ICALEO (2023)*, DOI: 10.48448/zk16-f979.
- [9] F. Bravo-Montero, D. Castells-Rufas, and J. Carrabina: *Opt. Laser Technol.*, 146, (2022) 107551.
- [10] E. Neiss, M. Flury, and J. Fontaine: *Proc. SPIE*, Vol. 7003, (2008) 70032.
- [11] S. Bruening, K. Du, M. Jarczyński, G. Jenke, and A. Gillner: *Procedia CIRP*, 74, (2018) 573.
- [12] S. Bruening, K. Du, and A. Gillner: *Phys. Procedia*, 83, (2016) 167
- [13] G. Jacob, L. Eng, S. Hamann, J. Hunter, T. Liu, H. Mizuno, and A. Payne: *Proc. SPIE*, Vol. 12414, (2023) 124140G.
- [14] S. Hamann: U.S. Patent 11933962 (2024).
- [15] J. Landry, S. Hamann, and O. Solgaard: *J. Biomed. Opt.*, 25, (2020) 106504.
- [16] Y. Ashida, S. Hamann, J. Landry, and O. Solgaard: *IEEE Photonics Technol. Lett.*, 32, (2020) 1291.
- [17] T. Sasaki, T. Kamada, and K. Hane: *J. Microbio. Robot.*, 32, (2020) 344.
- [18] O. Solgaard: U.S. Patent 11958738 (2024).
- [19] T. Liu, A. Payne, J. Hunter, G. Jacob, S. Yamashita, G. Myatt, L. Eng, Y. Hashimoto, H. Mizuno, Y. Fujisawa, and D. Hishitani: *Proc. 2021 Conference on Lasers and Electro-Optics (CLEO)*, (2021) AT4P.1.
- [20] D.M. Bloom: *Proc. SPIE*, Vol. 3013, (1997) 165
- [21] A. Payne, W. DeGroot, R. Monteverde, and D. Amm: *Proc. SPIE*, Vol. 5348, (2004) 76

(Received: June 14, 2024, Accepted: August 18, 2024)